# High-Dimensional Two-Photon Interference Effects in Spatial Modes

Markus Hiekkamäki* and Robert Fickler†
*Tampere University, Photonics Laboratory, Physics Unit, Tampere FI-33720, Finland*

(Received 7 November 2020; accepted 18 February 2021; published 22 March 2021; corrected 9 June 2022)

Two-photon interference is a fundamental quantum optics effect with numerous applications in quantum information science. Here, we study two-photon interference in multiple transverse-spatial modes along a single beam-path. Besides implementing the analog of the Hong-Ou-Mandel interference using a two-dimensional spatial-mode splitter, we extend the scheme to observe coalescence and anticoalescence in different three- and four-dimensional spatial-mode multiports. The operation within spatial modes, along a single beam path, lifts the requirement for interferometric stability and opens up new pathways of implementing linear optical networks for complex quantum information tasks.

DOI: 10.1103/PhysRevLett.126.123601

Two-photon interference at a beam splitter, i.e., Hong-Ou-Mandel (HOM) interference [1], is one of the most important effects in photonic quantum information science [2]. Its applications range from quantum computing [3], to cryptography [4] and from repeaters [5] to sensing [6], as well as quantum foundations [7]. Because of its importance, it has been studied with photons from different sources [8,9] and in different degrees of freedom (DOF) [10–12]. Domains that can encode high-dimensional quantum states, such as spatial, spectral, and temporal DOF, have attracted a lot of attention as they can be used to implement schemes with multiple input and output ports, i.e., multiports. Such linear optical networks are of importance for performing increasingly complex tasks in photonic quantum computing that require multiphoton interference [13–17].

Transverse-spatial modes, i.e., propagation invariant photonic structures that discretize the transverse-spatial domain, comprise a popular Hilbert space for encoding high-dimensional quantum states [18]. One prominent family of spatial modes is the Laguerre-Gaussian (LG) family that is defined by two quantum numbers, $\ell$ and $p$, describing the photons' azimuthal and radial structures, respectively. The azimuthal DOF has gained significant popularity as it is connected to the orbital angular momentum (OAM) of photons [19]. Benefits of encoding quantum states in photonic spatial structures include mature technologies for generating and detecting high-dimensional states, as well as intrinsic phase stability of complex superposition states, ensured by single beam-path operation.

In this Letter, we demonstrate two-photon interferences in multiple transverse-spatial modes. We use the technique of multiplane light conversion (MPLC) [20] to implement various spatial-mode unitaries, leading to different interference effects between two structured photons. We first observe bunching of photon pairs into the same spatial mode by implementing the direct spatial-mode analog of HOM interference using a two-dimensional "mode splitter." Utilizing the same setup and benefiting from the advantages spatial modes offer, we study various two-photon interferences in high-dimensional state spaces along with complex superposition states. The flexibility of our high-dimensional spatial-mode multiport further allows observing both coalescence and anticoalescence of photon pairs with three and four input and output modes. Our demonstration opens up paths to realize novel implementations and complement existing high-dimensional linear optical networks for quantum information science.

In the conventional HOM interference, photon bunching is obtained when two photons that are indistinguishable, i.e., perfectly overlapping in polarization, spatial structure, and time, are sent into a balanced beam splitter from separate inputs. While classically four different output situations are possible, only the two possibilities in which both photons exit through the same output port will remain after the interference [see Fig. 1(a)], which can be attributed to the bosonic nature of photons. A common way of assessing the quality of the interference is evaluating the change in coincident detections of the two exiting photons while scanning the temporal delay between them. This quality can be quantified with a visibility $V = |R_{\mathrm{cl}} - R_{\mathrm{qu}}|/R_{\mathrm{cl}} \in [0, 1]$ [21] between the classically expected rate $R_{\mathrm{cl}}$ and the rate $R_{\mathrm{qu}}$ observed due to quantum interference.

In our experiment, we replace the beam splitter acting on the paths with a mode splitter acting on the transverse-spatial modes of the photons. Hence, the photons bunch into the transverse-spatial modes, which is in contrast to previous quantum interference measurements, where spatial-mode overlap served as a *condition* for observing two-photon bunching into paths [26–30]. We note that in one recent experiment single-path two-photon interference between two spatially structured photons was observed, however, using polarization structures which limit the dimensionality to two [31].

 © 2021 American Physical Society

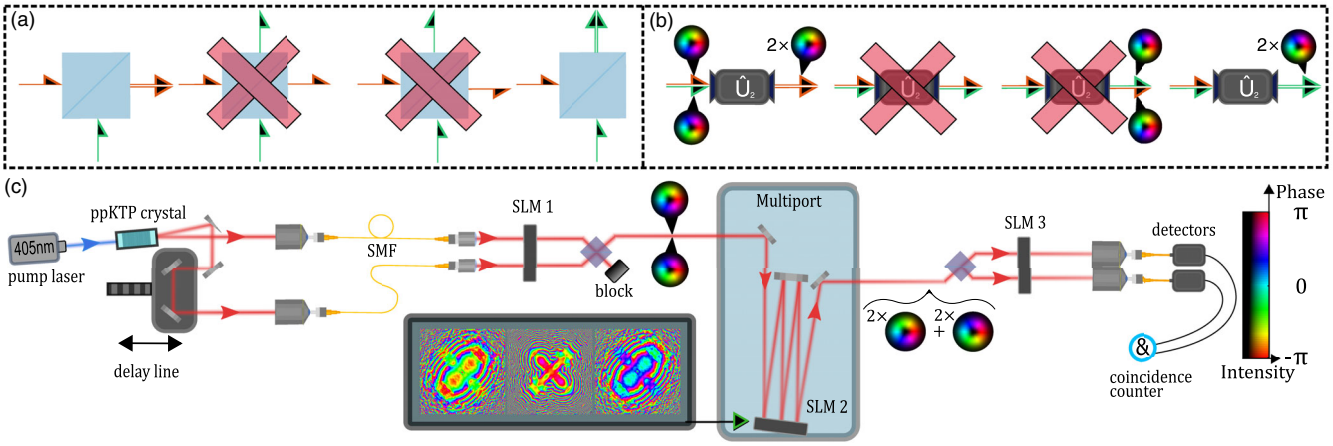


FIG. 1. Conceptual sketch of two-photon interference and the experimental setup. (a) Conventional HOM interference in a regular beam splitter between two paths. (b) Its spatial mode analog implemented with a mode splitter. (c) The setup used to demonstrate two-photon interferences in different mode splitters. Photon pairs are produced in a periodically poled potassium titanyl phosphate (ppKTP) crystal, adjusted in their temporal overlap using a delay line, and coupled into single mode fibers. Three spatial light modulators are used for spatial mode generation [22] (SLM1), unitary transformation [14] (SLM2), and measurement [23,24] (SLM3). Single photon detectors and a coincidence counter are used to detect the photon pairs. For more details, see the main text and Supplemental Material [25]. The two-dimensional color map shown in (c) is used in all of the figures.

To study HOM interference between two spatial modes, we prepare the photons in orthogonal OAM modes, i.e., one photon with $\ell = +1$ and the second having $\ell = -1$. Note that although our scheme would be able to transform any combination of spatial modes [14], we are only involving the OAM degree of freedom. Using the Fock-state notation $|n\rangle_\ell$, where $n$ is the photon number and the subscript labels the OAM value, we can write the input state as $|1\rangle_{-1}|1\rangle_{+1} = |1,1\rangle$. Analogous to the classic HOM interference, a balanced mode splitter unitary $\hat{U}_2$ transforms the two input modes into two equally weighted superpositions which leads, via interference, to the state

$$|\Psi_{2D}\rangle = \frac{1}{\sqrt{2}}(|0,2\rangle - |2,0\rangle), \tag{1}$$

if the two photons are perfectly indistinguishable in polarization, time, spectrum, as well as path [see Fig. 1(b) and the Supplemental Material [25] for more details]. This state is distinct from earlier spatial-mode interference experiments [26–30], as it is a so-called NOON state in a single optical path, which is a desirable state for quantum metrology tasks due to its increased phase sensitivity [32]. The single beam-path operation is similar to quantum interference with polarization [10,33], however, with the much larger state space that spatial modes offer. Thus, enabling more complex unitary transformations and a pathway to building single-path linear optical networks.

In the experiment [see sketch of the setup in Fig. 1(c) and Supplemental Material [25] ], we generate photon pairs using spontaneous parametric down-conversion, ensure their temporal overlap through a delay line in the path of one photon, and couple both photons into single mode fibers (SMF), thereby spatially filtering them to a Gaussian mode. Using a fiber beam splitter, we obtain an initial HOM visibility of $97.7\% \pm 0.2\%$ (see the Supplemental Material [25]). Note that for all visibility values given throughout the Letter, the errors denote a standard error calculated from a fit to the data. For more information on the specific function we fit to the data, see the Supplemental Material [25], which is partially based on the derivation in Ref. [34]. A few examples of these fits are shown in Fig. 2. We then imprint the desired spatial modes onto the photons using a spatial light modulator (SLM) and an amplitude and phase modulation technique to guarantee the best mode quality at the cost of loss (around 94%–99% loss per photon) [22]. Lossless schemes exist [35] but we abstain from using them due to their complexity. After imprinting the modes, the two photons are overlapped probabilistically with a balanced beam splitter. The input spatial modes are chosen to be orthogonal to avoid any interference in the combining beam splitter.

The photons are then input into the spatial-mode multiport, i.e., an MPLC setup, that we use to implement any unitary operation on the biphoton state. The three phase modulations in our MPLC setup, that define each unitary, are generated using free-space wavefront matching (WFM), which is described in more detail in the Supplemental Material [25], and an example code can be found in Ref. [36], and earlier works [14,37]. When generating these transformations, the pixelization and limited number of phase values (8 bit) of our SLMs are taken into account. Our 2D mode splitter achieved a simulated efficiency above 99% for a bandwidth of roughly 5 nm around the target wavelength. Importantly, out of the 1% loss, only a small fraction (1%) remains in our operating state space, i.e.,

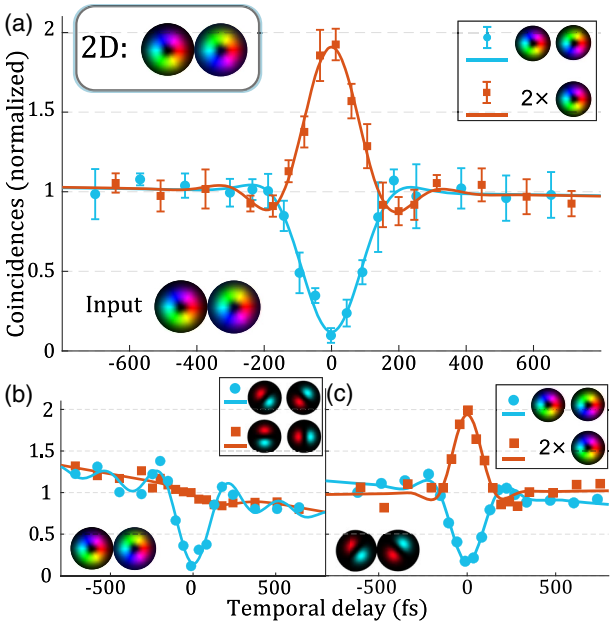


FIG. 2. Measurement of two-photon bunching in a two-dimensional mode splitter. (a) HOM-like interference visualized in Fig. 1(b). Insets show the input modes of both photons (lower left) and legends depict the mode pair they were projected on (upper right). (b) Interference data with the same input two-photon state projected onto two different MUBs. (c) Flipped scenario of (b), i.e., the input states are in a different MUB and projected onto the OAM basis. The mode splitter unitary $\hat{U}_2$ was the same in all three scenarios. The error bars are standard deviations calculated from multiple consecutive measurements and the curves are fits. In (b) and (c) the error bars were omitted for clarity and can be found in the Supplemental Material [25]. The change in the overall coincidence rates, especially visible in (b), is a result of decoupling over time.

contributes to errors. Note that this particular transformation for OAM modes $\ell = \pm 1$ resembles two rotated cylindrical lenses [38]. The simulated evolution of the photon's structure in the 2D transformation, with all the other utilized phase modulations, are displayed in the Supplemental Material [25].

After the two-photon state has been transformed through the mode splitter, the photons are probabilistically split into separate paths using another beam splitter. Their individual spatial modes are then measured using another phase modulation and SMF coupling followed by detection [23,24]. The signals of the detectors are fed into a time tagging unit, which registers coincident detections through temporal correlations. If the two-photon interference in spatial modes was successful, no coincidence counts will be detected when the photons are projected on orthogonal modes, i.e., using the projection operator $\hat{P}_{+1-1} = |1\rangle_{-1}|1\rangle_{+1}\langle 1|_{-1}\langle 1|_{+1} = |1,1\rangle\langle 1,1|$. Simultaneously scanning the temporal delay between the photons results in a dip in coincidence detections, identical to a classic HOM dip.

For the 2D mode splitter, we obtain a HOM-interference dip with a visibility $88.0\% \pm 3.8\%$, that is well above the classical limit of 50% [39]. When the two photons are projected onto the same state, i.e., $\hat{P}_{+1+1} = |0,2\rangle\langle 0,2|$, we observe an increase in coincidences due to bunching, i.e., a HOM bump, with a visibility $90.9\% \pm 4.5\%$. This change in the projection only requires changing one hologram on SLM3. Both results are shown in Fig. 2(a).

We then take advantage of a particular benefit of spatial modes and study the interference when generating and detecting superposition states, a task that is usually difficult to implement in other degrees of freedom. At first, we keep the photons in the same input state, but project them onto orthogonal states of the two other mutually unbiased bases (MUB), which we define as $|\Psi_{D/A}\rangle = 1/\sqrt{2}(|1,0\rangle \pm i|0,1\rangle)$ and $|\Psi_{H/V}\rangle = 1/\sqrt{2}(|1,0\rangle \pm |0,1\rangle)$. When projecting the photons onto the orthogonal states of the (D/A)-MUB, we again find an interference dip with a visibility of $85.6\% \pm 6.2\%$. However, when projecting both photons onto the (H/V)-MUB, no bunching is observed as both photons are transformed through the mode splitter into the eigenstates of this basis [see Fig. 2(b)].

To show that it is irrelevant whether we prepare or project onto superpositions, we then generate photons in the superposition states $|\Psi_A\rangle$ and $|\Psi_D\rangle$ but perform the projection measurements $\hat{P}_{+1-1}$ and $\hat{P}_{+1+1}$. The results are similar to the ones using no superposition states, with visibilities $84.0\% \pm 4.1\%$ and $93.8\% \pm 9.5\%$, for the dip and the bump, respectively [see Fig. 2(c)]. Note that, although the interference remains the same, the relative phase changes in the output state, allowing tuning of the obtained state.

To verify generation of the entangled state described in Eq. (1), we perform an entanglement witness test on the two postselected photons, which verifies nonseparability if the sum of the visibilities measured in at least two MUBs is larger than 1 [40–42]. From our measurements in all three MUBs, we obtain a witness value of $w = 2.2 \pm 0.1$, which is more than 11 standard deviations above the classical limit (see Supplemental Material [25] for details).

We then scale our state space to larger dimensions, i.e., study two-photon interferences in high-dimensional mode splitters. At first, we choose a balanced three-dimensional mode splitter $\hat{U}_3$ operating on the state space spanned by LG modes with $\ell = -1, 0, +1$. With this unitary, that splits the photons into an even superposition of all three spatial modes, different interference effects can be observed. For example, if we again send in the same input state, now written as $|\Psi\rangle = |1\rangle_{-1}|0\rangle_0|1\rangle_{+1} = |1,0,1\rangle$, we will not observe a perfect bunching. By measuring correlations using any of the projectors $\hat{P}_{+1-1}$, $\hat{P}_{+10}$, or $\hat{P}_{0-1}$, a HOM dip with a maximum visibility of 0.5 can be observed (see Supplemental Material [25]). Experimentally we measure visibilities of $39.7\% \pm 2.9\%$, $49.3\% \pm 3.1\%$,

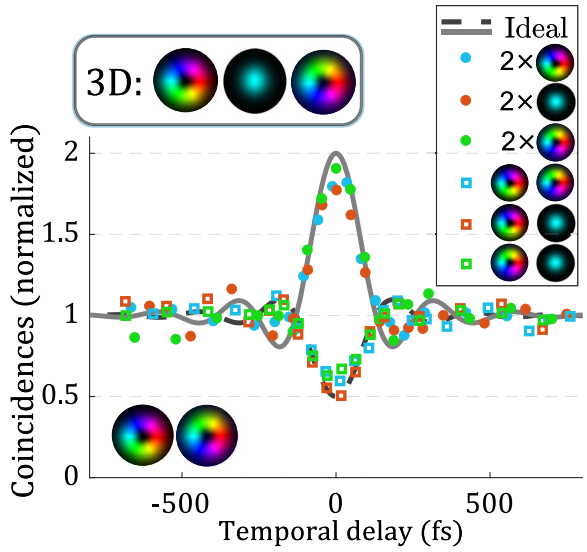


FIG. 3. Two-photon interference in a three-dimensional mode splitter. The two-photon input state, shown in the inset on the lower left, was sent into a balanced unitary $\hat{U}_3$. The resulting interference was measured when projecting the photon pair onto every combination of our initial basis states. The ideal curves were calculated from the theoretically expected visibilities and the two-photon properties measured at the source. The omitted error bars and more experimental details can be found in the Supplemental Material [25].

and $38.3\% \pm 2.8\%$. Similarly to the two-dimensional case, projecting both photons onto the same mode with $\hat{P}_{+1+1}$, $\hat{P}_{00}$, or $\hat{P}_{-1-1}$, results in a twofold increase in coincidences. The corresponding measurements lead to visibilities $84.3\% \pm 5.6\%$, $77.2\% \pm 4.8\%$, and $94.7\% \pm 7.2\%$, respectively (see Fig. 3). For the high-dimensional interference curves, we display ideal curves instead of fits, to keep the figure simple and compare the data to theoretically expected results. The imperfect visibilities are likely due to small misalignments and imperfections in the unitary implemented with only three phase modulations for these increasingly complex transformation. For completeness, we also confirmed that this three-dimensional unitary works with superposition states, which is shown in the Supplemental Material [25].

Naturally, scaling these effects into higher-dimensional state spaces, i.e., realizing linear optical networks, is important for quantum information applications [13–17]. However, this scaling also provides some fundamentally interesting effects that cannot be observed in a classical HOM setting, i.e., a two-dimensional system. One such effect is anticoalescence, where two-photon interference causes an increase in coincidences when projecting the biphoton state onto two orthogonal spatial modes, while still having a separable state as an input. In three dimensions, this phenomena can be observed if either the input states or the unitary is prepared in an unbalanced superposition basis. An example of the latter has been demonstrated using paths and an imperfect tritter [43], which could also be modeled as a lossy asymmetric beam splitter [44]. We demonstrate anticoalescence by exploiting the flexibility of our multiport, and compare the interference obtained with the balanced mode splitter $\hat{U}_3$ to an unbalanced unitary $\hat{U}_{\mathrm{Rot}+3}$, while keeping the same two-photon state $|1,0,1\rangle$ as input and output. As already shown in Fig. 3, for the balanced mode splitter $\hat{U}_3$ we observe coalescence. However, when using the unbalanced mode splitter $\hat{U}_{\mathrm{Rot}+3}$ we find an increase in coincidences with a visibility of $77.4\% \pm 6.4\%$ caused by anticoalescence [see Fig. 4(a)]. Because of the imperfections outlined earlier, our measured visibilities are slightly lower than the theoretically expected 100%. Because of the bosonic nature of photons, bunching is still the driving force of these interferences, which manifests as HOM dips when projecting on the two other orthogonal mode pairs (see Supplemental Material [25]). We further verified the same anticoalescence using the balanced unitary $\hat{U}_3$ and unbalanced superposition states, which can be found in the Supplemental Material [25].

When going beyond three dimensions, tuning the observed interference becomes easier since the mode splitter unitary can be kept balanced while changing its internal phases [43]. We demonstrate this tunability using a balanced four-dimensional mode splitter

$$\hat{U}_4 = \frac{1}{2}\begin{bmatrix} 1 & 1 & 1 & 1 \\ 1 & e^{i\varphi} & -1 & -e^{i\varphi} \\ 1 & -1 & 1 & -1 \\ 1 & -e^{i\varphi} & -1 & e^{i\varphi} \end{bmatrix}, \tag{2}$$

for which we adjust the internal phase values $\varphi$ to 0, $\pi/2$, or, $\pi$, corresponding to an anticoalescence, no interference, and coalescence, respectively. The chosen four-dimensional state space is spanned by the OAM modes with $\ell = \pm 2, \pm 1$. Although any two-mode combination of the mode set could have been used, we kept the same input state $|\Psi\rangle = |0\rangle_{-2}|1\rangle_{-1}|1\rangle_{+1}|0\rangle_{+2} = |0,1,1,0\rangle$ and projected on the same output state, i.e., $\hat{P}_{-1+1}$, as before to show that the change in interference only stems from the different unitary operation. In our measurements [shown in Fig. 4(b)] we obtained a visibility of $75.0\% \pm 6.1\%$ for $\varphi = 0$, no significant interference for $\varphi = \pi/2$ and a visibility of $63.2\% \pm 6.4\%$ for $\varphi = \pi$. While not being perfect, the obtained visibilities are above the classical limit, with at least 95% confidence. We again attribute the discrepancy between theory and experiment to the limitations of our small MPLC system performing more complex transformations. Already in simulations, the limited number of phase screens leads to an increase in mode-independent loss, around 27%–37%, and a slightly unbalanced mode splitter. Although MPLC setups have been implemented using a larger number of phase

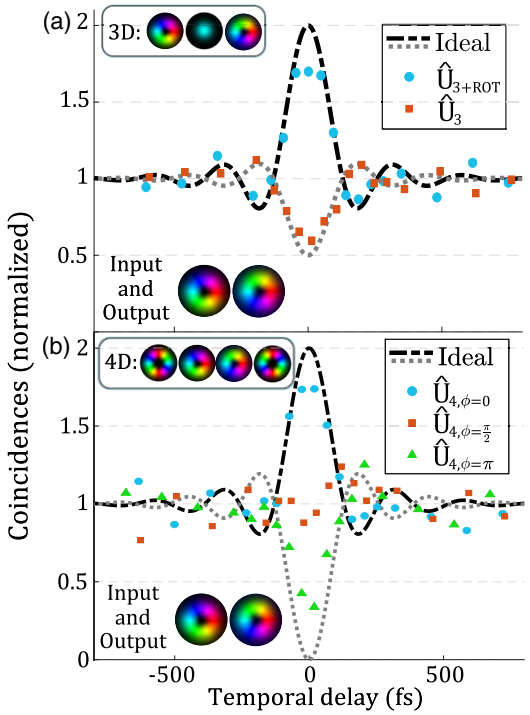


FIG. 4. Two-photon anticoalescence in a high-dimensional unitaries. The results in (a) show how imperfect coalescence in a three-dimensional state space can be changed to anticoalescence by changing to an unbalanced mode splitter unitary. Further, in (b), three different balanced four-dimensional mode splitters are used to tune the observed coalescence with the same input and output states. Definitions for the unitaries and error bars can be found in the Supplemental Material [25].

modulations on a single SLM [14,37], we refrained from doing so here due to the additional losses induced by every SLM reflection.

The multiphoton interference effects shown here, demonstrate that a reconfigurable spatial-mode multiport, implemented through MPLC, can be used in the quantum domain, opening up multiple new research avenues and quantum technological applications harnessing the benefits of spatial modes. The current limitation of our experimental scheme is the lossy method of generating the spatial modes [22] and the limited efficiency of our SLMs (75% efficiency per reflection), that limits the number of phase modulation planes. However, these limitations are only of a technical nature and can be tackled in the future with more expensive devices, e.g., high-quality deformable mirrors, and novel methods, e.g., lossless generation and detection of structured photons [35]. Because our scheme is intrinsically stable and can be fully automized [14], scaling to large mode numbers, i.e., the realization of large linear optical networks along a single path, seems feasible. Additionally, other input states, such as entangled states or multipartite states, could be used to investigate more complex multiphoton interferences. The well-controlled two-photon interference can further be applied in generating custom-tailored NOON states of spatial modes, studying complex quantum walks within the spatial-mode set [45], simplifying fundamental research endeavours such a high-dimensional multipartite entanglement [46], or applying spatial modes in complex quantum information tasks like photonic quantum processors [13,47], high-dimensional quantum teleportation [48], or Boson sampling [49].

The authors thank Marcus Huber, Mario Krenn, Shashi Prabhakar, and Lea Kopf for fruitful discussions. M. H. and R. F. acknowledge the support of the Academy of Finland through the Competitive Funding to Strengthen University Research Profiles (decision 301820) and the Photonics Research and Innovation Flagship (PREIN—decision 320165). M. H. also acknowledges support from the Magnus Ehrnrooth foundation through its graduate student scholarship. R. F. also acknowledges support from the Academy of Finland through the Academy Research Fellowship (Decision 332399).

*markus.hiekkamaki@tuni.fi
†robert.fickler@tuni.fi

[1] C. K. Hong, Z. Y. Ou, and L. Mandel, Measurement of Subpicosecond time Intervals Between Two Photons by Interference, Phys. Rev. Lett. **59**, 2044 (1987).
[2] F. Bouchard, A. Sit, Y. Zhang, R. Fickler, F. M. Miatto, Y. Yao, F. Sciarrino, and E. Karimi, Two-photon interference: The Hong-Ou-Mandel effect, arXiv:2006.09335.
[3] P. Kok, W. J. Munro, K. Nemoto, T. C. Ralph, J. P. Dowling, and G. J. Milburn, Linear optical quantum computing with photonic qubits, Rev. Mod. Phys. **79**, 135 (2007).
[4] F. Xu, X. Ma, Q. Zhang, H.-K. Lo, and J.-W. Pan, Secure quantum key distribution with realistic devices, Rev. Mod. Phys. **92**, 025002 (2020).
[5] S. Muralidharan, L. Li, J. Kim, N. Lütkenhaus, M. D. Lukin, and L. Jiang, Optimal architectures for long distance quantum communication, Sci. Rep. **6**, 20463 (2016).
[6] V. Giovannetti, S. Lloyd, and L. Maccone, Advances in quantum metrology, Nat. Photonics **5**, 222 (2011).
[7] D. Bouwmeester, J.-W. Pan, K. Mattle, M. Eibl, H. Weinfurter, and A. Zeilinger, Experimental quantum teleportation, Nature (London) **390**, 575 (1997).
[8] N. Somaschi, V. Giesz, L. De Santis, J. C. Loredo, M. P. Almeida, G. Hornecker, S. L. Portalupi, T. Grange, C. Antón, J. Demory *et al.*, Near-optimal single-photon sources in the solid state, Nat. Photonics **10**, 340 (2016).
[9] Y.-M. He, H. Wang, C. Wang, M.-C. Chen, X. Ding, J. Qin, Z.-C. Duan, S. Chen, J.-P. Li, R.-Z. Liu *et al.*, Coherently driving a single quantum two-level system with dichromatic laser pulses, Nat. Phys. **15**, 941 (2019).
[10] D. Branning, W. P. Grice, R. Erdmann, and I. A. Walmsley, Engineering the Indistinguishability and Entanglement of Two Photons, Phys. Rev. Lett. **83**, 955 (1999).
[11] A. Mohanty, M. Zhang, A. Dutt, S. Ramelow, P. Nussenzveig, and M. Lipson, Quantum interference

between transverse spatial waveguide modes, Nat. Commun. **8**, 14010 (2017).
[12] T. Kobayashi, R. Ikuta, S. Yasui, S. Miki, T. Yamashita, H. Terai, T. Yamamoto, M. Koashi, and N. Imoto, Frequency-domain Hong-Ou-Mandel interference, Nat. Photonics **10**, 441 (2016).
[13] J. Carolan, C. Harrold, C. Sparrow, E. Martín-López, N. J. Russell, J. W. Silverstone, P. J. Shadbolt, N. Matsuda, M. Oguma, M. Itoh *et al.*, Universal linear optics, Science **349**, 711 (2015).
[14] F. Brandt, M. Hiekkamäki, F. Bouchard, M. Huber, and R. Fickler, High-dimensional quantum gates using full-field spatial modes of photons, Optica **7**, 98 (2020).
[15] C. Reimer, M. Kues, P. Roztocki, B. Wetzel, F. Grazioso, B. E. Little, S. T. Chu, T. Johnston, Y. Bromberg, L. Caspani *et al.*, Generation of multiphoton entangled quantum states by means of integrated frequency combs, Science **351**, 1176 (2016).
[16] P. Imany, J. A. Jaramillo-Villegas, M. S. Alshaykh, J. M. Lukens, O. D. Odele, A. J. Moore, D. E. Leaird, M. Qi, and A. M. Weiner, High-dimensional optical quantum logic in large operational spaces, npj Quantum Inf. **5**, 59 (2019).
[17] S. Leedumrongwatthanakun, L. Innocenti, H. Defienne, T. Juffmann, A. Ferraro, M. Paternostro, and S. Gigan, Programmable linear quantum networks with a multimode fibre, Nat. Photonics **14**, 139 (2020).
[18] M. Erhard, R. Fickler, M. Krenn, and A. Zeilinger, Twisted photons: New quantum perspectives in high dimensions, Light Sci. Appl. **7**, 17146 (2018).
[19] L. Allen, M. W. Beijersbergen, R. J. C. Spreeuw, and J. P. Woerdman, Orbital angular momentum of light and the transformation of Laguerre-Gaussian laser modes, Phys. Rev. A **45**, 8185 (1992).
[20] G. Labroille, B. Denolle, P. Jian, P. Genevaux, N. Treps, and J.-F. Morizur, Efficient and mode selective spatial mode multiplexer based on multi-plane light conversion, Opt. Express **22**, 15599 (2014).
[21] G. Weihs, M. Reck, H. Weinfurter, and A. Zeilingerj, Two-photon interference in optical fiber multiports, Phys. Rev. A **54**, 893 (1996).
[22] E. Bolduc, N. Bent, E. Santamato, E. Karimi, and R. W. Boyd, Exact solution to simultaneous intensity and phase encryption with a single phase-only hologram, Opt. Lett. **38**, 3546 (2013).
[23] A. Mair, A. Vaziri, G. Weihs, and A. Zeilinger, Entanglement of the orbital angular momentum states of photons, Nature (London) **412**, 313 (2001).
[24] M. Krenn, M. Malik, M. Erhard, and A. Zeilinger, Orbital angular momentum of photons and the entanglement of Laguerre–Gaussian modes, Phil. Trans. R. Soc. A **375**, 20150442 (2017).
[25] See Supplemental Material at http://link.aps.org/supplemental/10.1103/PhysRevLett.126.123601 for additional data, extended discussion on methods, raw data, and detailed description of the setup.
[26] E. Nagali, L. Sansoni, F. Sciarrino, F. De Martini, L. Marrucci, B. Piccirillo, E. Karimi, and E. Santamato, Optimal quantum cloning of orbital angular momentum photon qubits through Hong–Ou–Mandel coalescence, Nat. Photonics **3**, 720 (2009).
[27] E. Karimi, D. Giovannini, E. Bolduc, N. Bent, F. M. Miatto, M. J. Padgett, and R. W. Boyd, Exploring the quantum nature of the radial degree of freedom of a photon via Hong-Ou-Mandel interference, Phys. Rev. A **89**, 013829 (2014).
[28] Y. Zhang, S. Prabhakar, C. Rosales-Guzmán, F. S. Roux, E. Karimi, and A. Forbes, Hong-Ou-Mandel interference of entangled Hermite-Gauss modes, Phys. Rev. A **94**, 033855 (2016).
[29] M. Malik, M. Erhard, M. Huber, M. Krenn, R. Fickler, and A. Zeilinger, Multi-photon entanglement in high dimensions, Nat. Photonics **10**, 248 (2016).
[30] Y. Zhang, F. S. Roux, T. Konrad, M. Agnew, J. Leach, and A. Forbes, Engineering two-photon high-dimensional states through quantum interference, Sci. Adv. **2**, e1501165 (2016).
[31] V. D'Ambrosio, G. Carvacho, I. Agresti, L. Marrucci, and F. Sciarrino, Tunable Two-Photon Quantum Interference of Structured Light, Phys. Rev. Lett. **122**, 013601 (2019).
[32] V. Giovannetti, S. Lloyd, and L. Maccone, Quantum-enhanced measurements: Beating the standard quantum limit, Science **306**, 1330 (2004).
[33] S. Slussarenko, M. M. Weston, H. M. Chrzanowski, L. K. Shalm, V. B. Verma, S. W. Nam, and G. J. Pryde, Unconditional violation of the shot-noise limit in photonic quantum metrology, Nat. Photonics **11**, 700 (2017).
[34] S. Prabhakar, C. Mabena, T. Konrad, and F. S. Roux, Turbulence and the Hong-Ou-Mandel effect, Phys. Rev. A **97**, 013835 (2018).
[35] M. Hiekkamäki, S. Prabhakar, and R. Fickler, Near-perfect measuring of full-field transverse-spatial modes of light, Opt. Express **27**, 31456 (2019).
[36] M. Hiekkamäki, S. Prabhakar, and R. Fickler, Wavefront matching code for transverse spatial mode conversion, https://doi.org/10.5281/zenodo.3570622 (2019).
[37] N. K. Fontaine, R. Ryf, H. Chen, D. T Neilson, K. Kim, and J. Carpenter, Laguerre-Gaussian mode sorter, Nat. Commun. **10**, 1865 (2019).
[38] M. W. Beijersbergen, L. Allen, H. E. L. O. Van der Veen, and J. P. Woerdman, Astigmatic laser mode converters and transfer of orbital angular momentum, Opt. Commun. **96**, 123 (1993).
[39] J. G. Rarity, P. R. Tapster, and R. Loudon, Non-classical interference between independent sources, J. Opt. B **7**, S171 (2005).
[40] R. Fickler, R. Lapkiewicz, S. Ramelow, and A. Zeilinger, Quantum entanglement of complex photon polarization patterns in vector beams, Phys. Rev. A **89**, 060301(R) (2014).
[41] S. Yu and N.-L. Liu, Entanglement Detection by Local Orthogonal Observables, Phys. Rev. Lett. **95**, 150504 (2005).
[42] O. Gühne and G. Tóth, Entanglement detection, Phys. Rep. **474**, 1 (2009).
[43] K. Mattle, M. Michler, H. Weinfurter, A. Zeilinger, and M. Zukowski, Non-classical statistics at multiport beam splitters, Appl. Phys. B **60**, S111 (1995).
[44] R. Uppu, T. A. W. Wolterink, T. B. H. Tentrup, and P. W. H. Pinkse, Quantum optics of lossy asymmetric beam splitters, Opt. Express **24**, 16440 (2016).
[45] M. Gräfe, R. Heilmann, M. Lebugle, D. Guzman-Silva, A. Perez-Leija, and A. Szameit, Integrated photonic quantum walks, J. Opt. **18**, 103002 (2016).

[46] M. Erhard, M. Malik, M. Krenn, and A. Zeilinger, Experimental Greenberger–Horne–Zeilinger entanglement beyond qubits, Nat. Photonics **12**, 759 (2018).

[47] A. Peruzzo, J. McClean, P. Shadbolt, M.-H. Yung, X.-Q. Zhou, P. J. Love, A. Aspuru-Guzik, and J. L. O'brien, A variational eigenvalue solver on a photonic quantum processor, Nat. Commun. **5**, 4213 (2014).

[48] Y.-H. Luo, H.-S. Zhong, M. Erhard, X.-L. Wang, L.-C. Peng, M. Krenn, X. Jiang, L. Li, N.-L. Liu, C.-Y. Lu *et al.*, Quantum Teleportation in High Dimensions, Phys. Rev. Lett. **123**, 070505 (2019).

[49] H. Wang, Y. He, Y.-H. Li, Z.-E. Su, B. Li, H.-L. Huang, X. Ding, M.-C. Chen, C. Liu, J. Qin *et al.*, High-efficiency multiphoton boson sampling, Nat. Photonics **11**, 361 (2017).

*Correction:* The inline equation in the fourth paragraph contained an error and has been fixed. The seventh sentence of the caption to Fig. 2 was misworded ("standard errors" should read "standard deviations"), and similar changes have been made to the captions to Figs. S5 and S8 of the Supplemental Material.